

**PREDICTION OF XV-15 TILT ROTOR
DISCRETE FREQUENCY AEROACOUSTIC
NOISE WITH WOPWOP**

Charles D. Coffen
and
Albert R. George

FDA-90-10

January 1990



Prediction of XV-15 Tilt Rotor Discrete Frequency Aeroacoustic Noise with WOPWOP

Charles D. Coffen
Graduate Research Assistant

Albert R. George
Professor

Abstract:

This report presents the results, methodology and conclusions of noise prediction calculations carried out to study several possible discrete frequency harmonic noise mechanisms of the XV-15 Tilt Rotor Aircraft in hover and helicopter mode forward flight. The mechanisms studied were thickness and loading noise. In particular, the loading noise caused by flow separation and the fountain / ground plane effect were predicted with calculations made using WOPWOP, a noise prediction program developed by NASA Langley. The methodology was to model the geometry and aerodynamics of the XV-15 rotor blades in hover and steady level flight and then create corresponding FORTRAN subroutines which were used as input for WOPWOP. This report describes the models and evaluates the simplifying assumptions made in creating them and presents the results of the computations. The computations lead to the following conclusions:

The fountain / ground plane effect is an important source of aerodynamic noise for the XV-15 in hover.

Unsteady flow separation from the airfoil passing through the fountain at high angles of attack significantly affects the predicted sound spectra and may be an important noise mechanism for the XV-15 in hover mode.

The various models developed in this study did not predict the sound spectra in helicopter mode forward flight. The experimental spectra indicate the presence of blade vortex interactions which were not modelled in these calculations.

The report indicates a need for further study and development of more accurate aerodynamic models, including unsteady stall in hover and blade vortex interactions in forward flight.

1 . Introduction:

The XV-15 Tilt Rotor has great potential for civil aviation applications because of its ability to emulate both helicopter and turboprop aircraft. The tilt rotor may become a more efficient mode of commuter transportation by reducing air traffic congestion at major airports via its ability to land and take off in densely populated urban centers. To be successful in this role, the XV-15 must prove itself to be a 'good neighbor' by meeting FAA standards for noise pollution. In effect, the future of the civilian tilt rotor is conditional on the aircraft's ability to operate quietly in take off, landing and the conversion corridor.

Theoretically the tilt rotor may be able to operate more quietly than a comparable helicopter in forward flight because the lift generated by the wings unloads the rotors which results in lower disk loadings and tip vortex strengths. In forward flight turboprop mode, the tilt rotor emits significantly less noise than a helicopter because of the absence of blade slap and other helicopter rotor phenomena. However, its unique rotor aerodynamics in hover and mixed flight mode cause strong rotor / wake interactions. These interactions emit high sound levels. Fortunately, the tilt rotor can fly in a wide variety of combinations of rotor tilt, rotor thrust, and wing lift. By studying the mechanisms of tilt rotor aerodynamic noise, it may be possible to define flight modes (combinations of rotor tilt, thrust, flap settings and forward velocity) and design modifications which minimize sound emission.

In this report two flight modes, hover and helicopter mode forward flight, were chosen for analysis because they reflect more critical aspects of tilt rotor take off and landing. Models were developed for these flight modes and applied in noise prediction calculations.

2. Survey of Procedure and Results:

Procedure:

The purpose of this study was to see if various aeroacoustic models used with WOPWOP¹ could predict the sound spectra obtained experimentally for the XV-15. WOPWOP is a noise prediction program developed by the NASA Langley Research Center to predict helicopter main rotor noise. WOPWOP predicts discrete frequency noise of helicopter rotors by employing the most advanced acoustic formulation of Farassat and allows for realistic helicopter blade motions and aerodynamic loadings. The blade motions and loadings must be input by the user, and the accuracy of the output depends almost entirely on the accuracy of this input.

The code requires the user to write three input subroutines in FORTRAN which describe the geometry and aerodynamics of the helicopter main rotor. WOPWOP also makes use of a name list data file which defines the operating conditions of the main rotor. The three input subroutines which we developed define a mathematical model of the XV-15 by making use of theoretical aerodynamics, data given in the Tilt Rotor Research Aircraft Familiarization Document², and experimental data for two dimensional airfoils. Many simplifying assumptions were made in creating this model which resulted in a relatively qualitative description of many aspects of tilt rotor aerodynamics.

Results:

All calculations were made for a single rotor operating at the specified conditions. Thus several corrections must be made when comparing predicted spectra with experimental spectra. The predicted spectra do not account for the presence of two rotors. The two signals could either reinforce or interfere with each other depending on the phasing of the acoustic pressure waves. The signals are assumed to be in phase in hover which leads to a 3 dB increase in predicted SPL levels. One must also note that the experimentally obtained spectra are 2 Hz bandwidth and were obtained with a ground plane microphone. Appendix A of reference 4 gives a full analysis of the various interference effects. Roughly, to compare experimental and predicted spectra, add 9 dB to the predicted value: 3 dB for 2 Hz bandwidth, 3 dB to double the acoustic pressure for two rotors and 3 dB to account for the ground plane microphone.

In hover, two different different aspects of the partial ground plane / fountain effect were studied: unsteady changes in attached flow lift and flow separation over stalled blade segments.

The wing's partial ground plane / fountain effect which is caused by the wing obstructing the down wash from the rotor, was modeled by decreasing the inflow velocity as the blade sweeps over the wing. Two models were used: the 'sharp' inflow variation was characterized by a sharp decrease in inflow velocity over the wing and the 'smooth' inflow variation was characterized by a gradual decrease in inflow velocity (see appendix D for details). The inclusion of the fountain effect in the WOPWOP calculations caused a significant increase in the predicted sound levels. The sharp fountain results were in good agreement with the experimental data (see figure 1 a-d) and were considerably higher than the smooth fountain results at higher frequencies. These results indicate that the high sound levels in the 400 to 2000 Hz frequency range can be attributed to the rapidly changing loads on the blade as it sweeps over the wing. The large variation between the results of the smooth fountain and sharp fountain models indicate a need to refine this model by actual measurement of inflow velocities over the wing section.

Separated flow about stalled sections of the rotor blade was also modelled. This phenomenon was included in the model because the XV-15 rotor is heavily twisted which may cause local separation over portions of the blade in hover. This was modeled by adapting the fountain hover model to include local regions of separated flow which increased in chordwise extent as the angle of attack was increased. Separated flow was modeled by relatively constant pressures in the separated region following the experimental data of reference 8. This modification resulted in significantly altering the noise spectrum (see figure 1 e-f). The scalloping of the spectra may be a result of the crude model developed to predict flow separation. The model neglects many of the aspects of rotor blade stall such as the dynamic transition from attached to separated flow. This lack of continuity is a result of modelling the two types of flow independently. The results do indicate that flow separation affects the XV-15 rotor noise and should be further studied with refinements to the model to include three dimensional and unsteady flow effects.

For helicopter mode forward flight, the flow separation model was also included in the aerodynamic model for the XV-15. The results of forward flight noise prediction calculations show poor agreement with the experimental results (see figures 2 - 4). The fundamental harmonic is high by approximately 20 dB in all cases. For the calculations without blade stall effects the higher harmonics are low by some 20 dB. Calculations with the stall model give SPL values 20 dB higher than experimental spectra at all frequencies. The conclusions that can be made from these results are that flow separation may be a secondary sources of aerodynamic rotor noise for the XV-15 in helicopter mode forward flight and that better models needs to be

developed. This is especially true since the model used here failed to predict the spectra for the non BVI case (figure 2). A model that includes blade vortex interactions also needs to be developed.

3. Description of the Aerodynamic Models:

The following describes the FORTRAN subroutines used as input for WOPWOP. The organization of this description parallels the WOPWOP user's manual by defining the variables as they appear in the manual.

3.1 Subroutine FUNE2:

This routine defines the main rotor blade geometry in the radial direction. The parameters of interest in this routine are the geometric twist of the blade, chord width, thickness and camber.

Geometric Twist:

The geometric twist of the blade is defined by two linear functions of radial position. One function covers the rotor blade from $r=0$ to $r=1/2R$ and the other covers the rotor blade from $r=1/2R$ to R . These two linear functions are taken without change from data supplied by Bell, 'XV-15 Blade Properties'. The derivative of the variation of twist with radius is defined by the slope of the linear function.

Pitch Change Axis:

Two other geometric quantities which require definition are the perpendicular distance from the chord line to the pitch change axis and the distance from the pitch change axis to the leading edge of the blade section. The pitch change axis distance was assumed to be zero over the span of the blade and the leading edge distance was assumed to be 25% of the chord and was taken to be negative. These assumptions are made from the sample routines included in the WOPWOP manual as no data was available to accurately define these quantities.

Chord:

The chord of the blade section was defined as a function of radius and varies linearly from 18.2 inches at the theoretical root to 14 inches at 25% of the radius. From this point to the blade tip the chord was a constant 14 inches. This data was taken from 'XV-15 Blade Properties' provided by Bell.

Maximum Thickness Ratio:

The maximum thickness ratio of the blade section, thickness/chord, was defined by calculating a linear function of radius from the Bell airfoil data given for 14 radial stations in

'XV-15 Blade Properties'. The maximum thickness ratio varied from 35% at the theoretical root to 8% at the tip.

Maximum Camber Ratio:

The maximum camber ratio of the blade section, camber/chord, is defined by the airfoil section at each radial station. The airfoil section is given by Bell in 'XV-15 Blade Properties' for 14 stations. Every section is a 64 series airfoil. The data states that design coefficients, c_l , are assumed to vary linearly between stations. The maximum camber ratio is defined as the camber ratio times the design lift coefficient divided by the ideal coefficient of lift for a 64 series airfoil (see reference 3). The design lift coefficient was found by linear interpolation between values given at the 14 radial stations.

3.2 Subroutine FUNE2O:

This subroutine defines the chordwise geometry of the rotor blade in terms of radial and chordwise location.

Camber:

The camber is defined as the distance from chord line to camber line divided by the maximum camber displacement and is expressed as a fifth order polynomial fit to the data points found in reference 3, p.385. The function is multiplied by a correction factor for design lift coefficient based on the radial station location of the blade element as described above for maximum camber distance in FUNE2.

Thickness:

The thickness is defined as the distance from camber line to upper or lower surface divided by the maximum thickness. This distance is measured perpendicular to the chord line. The thickness at a given chordwise and radial location is calculated by chordwise and radial interpolation from defined data points. Data for 64 series airfoils of various thicknesses is tabulated in reference 3, p. 347 - 353 in terms of chordwise position. These tables were used to create a two dimensional set of data points (radial and chordwise frame of reference) from which the thickness at a given point on the blade can be extrapolated by linearly interpolating between four data points surrounding the point of interest. Five radial stations were selected to create the mesh with airfoils of 8%, 12%, 18%, 28%, and 35% thickness. The only significant

approximation was that data had to be created for 28% and 35% thick airfoils. This was done by linearly scaling the thickness data of a 21% thick airfoil. This approximation is reasonable as the data given by reference 3 varies approximately linearly with thickness for 64 series airfoils. A more rigorous mathematical model of the rotor blade should include more airfoil sections and actual data for the thicker airfoils.

Chordwise Derivatives:

The derivative of the camber with respect to chord was calculated by taking the derivative of the polynomial function. The derivative of thickness with respect to chord was calculated using a finite difference method over a 1% length of chord. The derivative is calculated over a 1/2% length of chord at the leading and trailing edges.

3.3 Subroutine FUNPSI:

This subroutine describes the pressure distribution on the blade surface as a function of radial, chordwise and azimuthal position. This is the most complicated of the input routines and requires several assumptions and qualitative descriptions of the complicated three dimensional flow about a rotor blade in hover and forward flight. The method of computing the pressure at a point on the rotor blade was similar for hover and forward flight. The point is defined by its radial, chordwise and azimuthal positions. From these three coordinates, the angle of attack and relative velocity is calculated for the blade element containing the point. The pressure coefficient is then determined by the velocity addition method of reference 3.

Hover Relative Velocity and Angle of Attack:

In hover, the angle of attack is equal to the sum of the collective pitch, blade twist and inflow. The twist is known from subroutine FUNE2. The inflow was assumed constant such that:

$$V_{in} = \sqrt{\frac{\text{Thrust}}{2 \cdot \text{density} \cdot \text{disk area}}}$$

The inflow angle is calculated as:

$$\tan^{-1}\left(\frac{V_{in}}{\text{radial velocity}}\right).$$

For some hover computations, the inflow was made to vary as a half wave sinusoid when the blade element passed over the wing of the XV-15. The inflow was 80% - 100% of the constant inflow value, 80% as the element reached the center of the wing (see appendix D). This

sinusoidal variation was meant to model the 'fountain / ground plane effect' created by the recirculating inflow caused by the wings obstructing the outflow from the rotor.

In hover, the collective was found by adjusting the collective angle until WOPWOP calculated the thrust required to match the hover value of C_T given in reference 4. This procedure provided radially varying angles of attack in agreement with hover data provided by Bell.

The relative velocity of the blade element was simply the radial distance from the hub times the rotor rate of rotation, $V = \Omega \cdot r$.

Forward Flight Relative Velocity and Angle of Attack:

In forward flight, calculation of the angle of attack and apparent velocity was fairly complicated because the flapping and feathering coefficients were not known. This calculation is further complicated as both the rotors and the wings are providing lift. In order to approximate the blade motion, a FORTRAN routine was written which employs the analysis of reference 5 (see appendix B). In doing so, several assumptions were made which result in a significant quantitative loss of accuracy:

1. The reverse flow region of the blade on the retreating side was ignored by setting all negative velocities to zero. Hence the negative lift was not accounted for.
2. Blade flapping was assumed to be negligible for this group of calculations and flapping coefficients were set equal to zero.
3. The angle of attack of the tip path plane was assumed to be equal to 90 minus the nacelle angle. This follows from the assumption that there was no flapping.
4. Root cut out and tip loss factors were not included which results in the calculations being based on blade span longer than actual.
5. The rotor was assumed to be hinged at the center of the hub.

The three dimensional flow was modeled as the integration of two dimensional flows over the span of the blade. Thus the total lift in the analysis is calculated via incremental lift in which it is assumed that $c_l = 6 \cdot \alpha$.

In reference 5 the blade motion is calculated by solving for the trim control angles of a rotor in steady level flight such that the aerodynamic, weight, inertial, and centrifugal forces acting on the blade element are balanced and C_T is known. This analysis is for a helicopter rotor in forward flight and it should be noted that the contribution to lift by the wing is accounted for by basing the calculations on the known thrust of the rotor.

The results of the analysis provide a good mathematical description of how the angle of attack of a blade element varies with azimuthal position in forward flight. The collective was increased by 5 degrees above its calculated value to match the lift calculated by WOPWOP with the known value. Comparing the results of this method with data provided by Bell show good agreement though the azimuthal variation of calculated angles of attack were off by a few degrees in some cases (figure 5 a-b). This result is to be expected as the analysis of reference 5 does not account for loss of lift due to stall at high angles of attack, root cut out and tip loss, or negative lift in the reverse flow region. Qualitatively the variation was quite accurate. Because a constant error in angle of attack results in a constant pressure error, the noise calculations should not be greatly affected. The noise generated by an airfoil depends largely on changing pressure distributions as the blade element changes angle attack. These changes are accurately reflected by the model used here for calculating the angle of attack.

Setting the flapping coefficients to zero may alter the predicted noise signature as this value changes the thickness noise significantly in the low harmonics.

Pressure Distribution Calculation:

The pressure distribution about the airfoil was calculated using the velocity addition method of reference 3 outlined in appendix A. This method is based on adding velocity increment ratios due to camber, thickness and angle of attack in order to find the total velocity ratio at a point on an airfoil. The data for this technique was tabulated for 64 series airfoils in reference 3 pp. 346-353. As with the thickness calculations, data had to be estimated for 28% and 35% thick airfoils by scaling data from thinner airfoils. The results of this scaling are questionable as the velocity addition method may be inaccurate for thick airfoils. However, pressure distributions calculated by this method appear to be qualitatively correct and agree well with pressure distributions calculated using a panel method⁷ for thin airfoils at low angles of attack.

Pressure Distribution Correction for Angles of Attack Greater than 10°:

One obvious failing of the velocity addition method is that it does not account for stall or flow separation. A very rough qualitative flow separation and stall correction was included in the model. Stall represents a significant source of aerodynamic noise (see reference 6) and significantly affects WOPWOP output.

The flow separation calculation was based on a qualitative approach. Data for a 64A airfoil of 10% thickness was obtained for angles of attack ranging from -6° to 28° (see reference 8). An attempt was made to create a mathematical model which reflected the pressure distribution of the 64A airfoil as separation occurred. At angles of attack greater than 10 degrees, the values of C_p were adjusted to produce distributions resembling the plots obtained for 64A data (see appendix C).

This crude method of calculating the pressure distribution about an airfoil in a separated flow lacks concrete theoretical basis but does model the effects of separation which become more severe with increasing angles of attack in a manner similar to 2-D steady flow experiment. Also, the use of 2-D steady flow airfoil data in modeling the turbulent separated flow around a three dimensional rotor blade has other failings such as neglecting the effect of dynamic stall and delayed stall on the pressure distribution of a blade section, and the three dimensional aspects of the flow including how separated flow over a stalled airfoil affects the flow over un-stalled sections of the blade. But without complex and CPU-consumptive CFD calculations, this is the most reasonable way to create a first try at a qualitatively accurate mathematical model of the pressure distribution about the XV-15 rotor in hover and forward flight. Some sample pressure distributions of this model compared to the experimental data of reference 8 can be found in figures 6 a - f. As the dynamics of how the blade stalls significantly affects the noise spectrum, a more precise model is necessary to more accurately predict rotor noise. Further investigation into the effects of stall should include the effects of dynamic stall, three dimensional flow, and accurate airfoil data pertaining to the 64 series airfoils used on the XV-15 rotor blade.

Miscellaneous:

The above pressure distribution is corrected for compressibility by the Prandtl Glauert compressibility correction.

The time derivative of the pressure was calculated using a finite difference method over one degree of azimuth ($\Delta t = \Delta \psi / \omega$).

The name list specifies the operating conditions of the main rotor including the location of the microphone, forward speed, rotor speed and blade motion coefficients. The inputs for the operating conditions were obtained from the experimental cases of hover and forward flight. The blade motion coefficients are defined by the results of the analysis of reference 5 which calculates these coefficients in the process of computing the blade element angle of attack in forward flight.

The blade lagging coefficients were set to zero (no lagging motion) as no information was available to define the lagging motion.

The above three subroutines and name list represent a mathematical model of the geometry and aerodynamics of the XV-15 rotor. The results from using these with WOPWOP has provided some interesting results regarding the effects of stall and the fountain effect. They also show that the discrete noise spectrum in forward flight cannot be fully attributed to stall and is most likely a result of blade vortex interactions.

4. Conclusion:

The results of computations made with the above mathematical model indicate that the partial ground plane / fountain effect is a significant contributor to the discrete frequency rotor noise of the XV-15 in hover. Unsteady blade stall in hover due to the fountain effect is probably a secondary source of noise for the XV-15, though more so than for helicopters because of its highly twisted blade and the presence of the wing effect which causes the blade element angle of attack to increase sharply as it passes over the wing. Computations including the fountain effect predicted OASPL of 5 dB higher and SPL levels 40 dB higher (frequencies greater than 500 Hz) than computations without the fountain effect (figure 1 b-d). This result indicates that tilt rotor noise in hover can be reduced by reducing the effects of the fountain / ground plane caused the presence of the wing in the rotor out flow.

Blade stall as modelled here was seen to have an effect on the noise spectrum in both hover and forward flight and should not be neglected in future studies. The approximate stall model showed that stall increases aerodynamic noise because of non-constant blade loadings. Blade stall and turbulent separated flow over blade elements passing through the fountain should be the topic of further studies as this has proved to be a significant source of tilt rotor noise.

Finally, this study has shown that the aerodynamics of tilt rotor helicopter mode forward flight are especially difficult to model accurately and that a qualitative analysis was all that was possible. This model includes blade stall, realistic blade motions, and representative angle of attack and relative velocity calculations. However, this model indicates (through poor agreement with experiment) that blade stall and the time varying blade loadings associated with these loadings are not the main source of aerodynamic noise under forward flight conditions. Further study must be made into other noise sources, such as BVI, in order to develop an accurate model.

Appendix A

Explanation of Coefficient of Pressure Calculation:

This calculation is based on the velocity addition method of Abbott and Von Doenhoff presented in Theory of Wing Sections³. The theory of thin wing sections shows that the loading component of the pressure distribution of a thin section may be considered to consist of a basic distribution at the ideal angle of attack due to camber, a distribution proportional to the angle of attack as measured from the ideal angle of attack, and an additional distribution associated with the basic thickness form (symmetrical section) at zero angle of attack (pp. 75-76)

The load at a chordwise position is caused by a pressure difference between the upper and lower surfaces. It is assumed that the velocity increment on one surface is equal to the velocity decrement on the other surface. Using the method of velocity addition, the coefficient of pressure, $S = 1 - C_p$, can be calculated by adding the velocity increment corresponding to camber, $\Delta v/V$, and the velocity increment corresponding to angle of attack, $\Delta v_a/V$, to the velocity increment due to the basic thickness form, v/V .

$$S = \left(\frac{v}{V} \pm \frac{\Delta v}{V} \pm \frac{\Delta v_a}{V} \right)^2$$

Values of the ratios corresponding to one value of x/c are added together and the resulting value of the pressure coefficient S is assigned to the surface of the wing section at the same value of x/c . The values of $\Delta v_a/V$ and $\Delta v/V$ are added on the upper surface and subtracted on the lower surface. In this way a pressure distribution about an airfoil can be calculated where $C_p = 1 - S$.

A correction must be made as the pressure distribution is being calculated for an arbitrary c_l , not c_{li} . For this reason, the ratio $\Delta v_a/V$ must be corrected by multiplying by a factor $f(\alpha)$. As a first approximation:

$$f(\alpha) = (c_l - c_{li}) / c_{l0}$$

$$c_l = c_{li} + dc_l/d\alpha (\alpha - \alpha_i)$$

$$f(\alpha) = dc_l/d\alpha \cdot (\alpha - \alpha_i) / c_{l0}$$

and c_{l0} is taken to be unity.

The ratio $\Delta v/V$ must also be corrected as the value of the design c_l will be higher than c_{li} of the camber line by an amount dependent on the thickness ratio of the basic thickness form. This discrepancy is caused by applying the values of $\Delta v/V$ obtained for the mean line to the sections of finite thickness where v/V is greater than unity over most of the surface. So $\Delta v/V$ is multiplied by the design lift coefficient divided by the design lift coefficient of the mean line.

This method is known to be very accurate for thin airfoils with thin boundary layers and low drag coefficients. However, it is possible that the data estimated for the 28% and 35% airfoils may be significantly in error.

The velocity addition method was applied to the input subroutine as no empirical data for the XV-15 rotor was available and any type of panel method would be inefficient. The velocity addition method allows the fast and accurate calculation of the the pressure coefficients on the upper and lower surfaces at discrete chordwise locations at angles of attack such that separation is not a problem.

Data for the 64 series thickness forms are tabulated in Appendix 1 and 2 of reference 3. These tables were entered as data statements in FORTRAN subroutines. Data had to be estimated for the 28% and 35% airfoils from a 21% airfoil. v/V was found by using equation 6.5 of reference 3.

$$\left(\frac{v}{V}\right)t_2 = \left[\left(\frac{v}{V}\right) - 1\right] \cdot \frac{t_2}{t_1} + 1$$

$\Delta v_a/V$ was estimated by scaling the first 5% of the chord exponentially from several thinner airfoils and then using the same values as are given for the 21% airfoil. These values were used as it was noted qualitatively that these values changed little as thickness increased. As noted previously the velocity addition method may be imprecise for thicker airfoils, the pressure distributions about these airfoils can be considered as approximate.

This tabulated data represents a two dimensional array of velocity ratios from which the desired values at a specific point on the rotor blade can be calculated by linearly interpolating from four surrounding defined data points. In this way a call to the FORTRAN subroutine identifies the four data points and then interpolates to produce the velocity ratios at the desired point.

Appendix B

Angle of Attack and Relative Velocity Calculations for Forward Flight:

In order to define the pressure distribution on a blade element of a rotor in forward flight, the blade element angle of attack must be known. As in hover, the angle of attack is equal to the blade pitch and inflow angle. However, deriving a simple calculation for the inflow of a rotor blade which includes forward motion, rotation, flapping and feathering requires many simplifying assumptions. What follows is not meant to be a rigorous explanation of helicopter aerodynamics but a brief synopsis of the analysis of reference 5 leading to the equations used in the FORTRAN subroutine.

The velocity perpendicular to the leading edge, tangent to the chord of the blade element, U_T is given by:

$$U_T = \Omega r + V \sin\Psi$$

and can be expressed in terms of the rotor's tip speed ratio, μ :

$$U_T = \Omega R \left(\frac{r}{R} + \mu \sin\Psi \right)$$

The motion of the blade flapping can be expressed as an infinite Fourier series of which only the first three terms are important (a_0 is defined as the coning angle):

$$\beta = a_0 - a_{1s} \cos\Psi - b_{1s} \sin\Psi$$

The motion of the blade feathering or cyclic pitch can also be expressed as an infinite Fourier series plus two constant terms, twist and collective pitch. Only the first three terms are retained.

$$\Theta = \Theta_0 + \Theta_1 \frac{r}{R} - A_1 \cos\Psi - B_1 \sin\Psi$$

Having defined the blade motion, the inflow angle can be defined in terms of $\tan^{-1}(U_P/U_T)$. By resolving velocity vectors into components and adding, the following expression can be derived for angle of attack:

$$\begin{aligned} \alpha = & \frac{1}{\frac{r}{R} + \mu \sin\Psi} \left\{ \frac{r}{R} \left[\Theta_0 + \Theta_1 \frac{r}{R} (A_1 - b_{1s}) \cos\Psi - (B_1 + a_{1s}) \sin\Psi \right] \right. \\ & - \frac{V_1}{\Omega R} \left(1 + \frac{r}{R} \cos\Psi + \mu [\alpha_{TPP} + \Theta_0 + \Theta_1 \frac{r}{R} \sin\Psi] \right. \\ & \left. \left. - a_0 \cos\Psi - (A_1 - b_{1s}) \sin\Psi \cos\Psi - (B_1 + a_{1s}) \sin^2\Psi \right\} \right\} \end{aligned}$$

When α is expressed in this form, the combinations of cyclic pitch and flapping, $(A_1 - b_{1s})$ and $(B_1 + a_{1s})$, occur as primary variables which is a consequence of the equivalence of flapping and feathering.

$(A_1 - b_{1s})$ and $(B_1 + a_{1s})$ for a rotor blade in steady level forward flight can be calculated by employing a force balance and setting the rolling and pitching moments to zero. (The rotor blades are assumed to be hinged at the hub and thus cannot support a moment.) By setting the rolling moments to zero:

$$B_1 + a_{1s} = \frac{\mu}{1 + \frac{3}{2}\mu^2} \left[\frac{8}{3}\Theta_0 + 2\Theta_1 + 2\lambda' \right]$$

and by setting the pitching moments to zero:

$$A_1 - b_{1s} = \frac{\left(\frac{4}{3}\mu a_0 + \frac{v_1}{\Omega R} \right)}{1 + \frac{\mu^2}{2}}$$

The collective pitch, Θ_0 , can be calculated by knowing the value of C_T/σ and is adjusted to produce the correct thrust:

$$\Theta_0 = \frac{\frac{4}{a} \left(1 + \frac{3}{2}\mu^2 \right) C_T/\sigma - \frac{1}{2} \left(1 - \frac{3}{2}\mu^2 + \frac{3}{2}\mu^4 \right) \Theta_1 - \left(1 - \frac{\mu^2}{2} \right) \lambda'}{\frac{2}{3} - \frac{2}{3}\mu^2 + \frac{3}{2}\mu^4} + 5 \text{ deg.}$$

The coning angle can be found by setting all the blade bending moments caused by aerodynamic, weight, inertial and centripetal forces to zero at the hinge:

$$a_0 = \frac{2}{3} \gamma \frac{C_T/\sigma}{a} - \frac{\frac{3}{2}gR}{(\Omega R)^2}$$

In this analysis, the angle of attack of the tip path plane, a_{TPP} , is used instead of the angle of attack of the plane perpendicular to the shaft.

$$a_s = a_{TPP} - a_{1s}$$

For the case of the XV-15, the assumption is made that $a_s = a_{TPP}$ (90 - nacelle angle) and a_{1s} is equal to zero.

Also, the lateral flapping, b_{1s} , is that required to trim the rotor for external rolling moments such as would be produced by tail rotor forces or center of gravity offset. As the XV-15 has no tail rotor and the center of gravity is balanced by two main rotors, it is assumed that b_{1s} is equal to zero. This and the above assumption lead to the conclusion that flapping can be

ignored in steady forward flight, though this would be a poor assumption during a flight maneuver. The above equations can be solved for feathering coefficients which are used as input data in the name list ($A_1 = -1.9^\circ$ & $B_1 = 2.5^\circ$ for the forward flight case studied here).

v_1 is the induced velocity which can be defined as follows from the momentum equation:

$$v_1 = \frac{\Omega R C_T}{\mu} \frac{1}{2}$$

λ' is the inflow ratio with respect to the tip path plane and is defined as follows:

$$\lambda' = \mu \alpha_{TPP} - v_1 / \Omega R$$

As stated in the main text, many simplifying assumptions have been made in order to keep the calculations simple and quick. These assumptions would be inadequate if used in designing a helicopter, however the purpose here is to provide rudimentary numerical input which describes the the changing angle of attack of a XV-15 rotor in forward flight. Hence this qualitative result should be adequate to determine trends in the noise calculations.

Appendix C

Flow Separation Estimation:

One of the most important aspects of the XV-15 rotor design is that the blade twist is designed to be reasonably efficient in forward flight as well as in hover and mixed flight modes. Most helicopters are designed with 5 - 12 degrees of twist while the XV-15 has 40 degrees of twist. One important effect of this highly twisted blade is that in hover and helicopter mode, a significant portion of the blade may experience stall and or flow separation. According to Richards and Mead (reference 6), blade stall is a strong source of aerodynamic noise. As the XV-15 rotor blade probably experiences stall, it should be accounted for in the model. This means that the results of the velocity addition method had to be somehow modified at angles of attack where the blade element would experience flow separation. This phenomenon was modeled by defining four ranges of angles of attack where the flow would be defined by different mathematical models, depending on the amount of separation that would be expected. Separated flow was modeled by defining regions of separation which increase in chordwise extent as the angle of attack is increased. These ranges and models were defined by a qualitative analysis of 64A series airfoils at angles of attack ranging from -6° to $+28^\circ$ found in reference 8.

In the range from -10° to $+10^\circ$ the velocity addition method of reference 3 is used without modification. This assumes that in this range, lift varies linearly with angle of attack.

From $\pm 10^\circ$ to $\pm 15^\circ$, the flow is assumed to separate from the trailing edge on the upper surface. This is modeled by creating a curve fit of the form $C_p = \Delta C_p * Q^{\text{exp}}$ where exp is a negative number and ΔC_p is the difference between C_p at 1% chord on the upper surface and C_p at the trailing edge, and Q is the non-dimensionalized chordwise position. The trailing edge value of C_p is made to vary linearly between -0.3 and -0.8 as the angle of attack increases from 10° to 15° . On the lower surface, the values of C_p are defined up to the 70% chord by the velocity addition method. From the 70% chord to the trailing edge, C_p varies quadratically from $C_p(Q = 0.7)$ to $C_p(\text{trailing edge})$.

From $\pm 10^\circ$ to $\pm 22^\circ$ a separation correction must be made at the leading edge as the velocity addition method gives higher and higher values of C_p at the leading edge as the stagnation point moves further back on the lower surface. According to the experimental data, in this range of angles of attack, C_p at the leading edge is approximately -0.8 and changes rapidly to a 'maximum' value between -4 and -0.8 (as alpha increases from 15° - 22°) at 1% of the chord. This is modeled mathematically as a straight line between the leading edge and 1% of the chord.

This linear curve fit is theoretically and experimentally inaccurate and leads to a discontinuity in slope. However, WOPWOP does no computations with the chordwise derivative of C_p and requires C_p at only discrete points as input. Thus the linear curve fit satisfies the qualitative aspects of the model without grossly affecting any quantitative aspects of the computation. The value of C_p on the lower surface must be corrected in order to match the pressures on the upper and lower surfaces at the leading edge. C_p on the lower surface is forced to -0.8 at the leading edge and is then increased linearly until the value of C_p calculated by the velocity addition method becomes more realistic, i.e. greater than $-0.8 + 10*Q$. This approximation is used for less than 1% of the chord on the lower surface and the number of points in this range requiring calculation in calls from WOPWOP is few and may be none depending on the number of chordwise points WOPWOP requires. From the 1% chord to the trailing edge the calculations are carried out as for the $\pm 10^\circ$ to $\pm 15^\circ$ range. The only differences are that the value of C_p at the 1% chord are determined by qualitative analysis of experimental data (reference 8) instead of by the velocity addition method which would give unrealistically high values. Also the value of C_p at the trailing edge is set to a constant -0.8 in keeping with the experimental data. For angles of attack greater than $\pm 22^\circ$, the value of C_p is set to -0.8 over the entire upper surface. C_p on the lower surface is calculated identically as in the $15^\circ - 22^\circ$ range.

The above mathematical model is a result of combining the Abbott and Von Doenhoff thin airfoil model with a qualitative analysis of experimental data of a similar airfoil at high angles of attack from reference 8.

Appendix D

Plane / Fountain Effect:

Substantial loading noise is produced on the tilt rotor blades due to the strong effect of the wing on the flow in the rotor plane in hover. The model developed for WOPWOP input was based on analysis by reference 4. The velocity distribution through the fountain flow was estimated based on smoke flow video tapes, photographs and correlated CFD results⁹. The results of this analysis were used in the creation of a mathematical model. This model defines the width of the the affected region to be approximately equal to 1/3 to 1/2 the wing chord and the ground effect to cause a 20% reduction in the inflow velocity over the wing. As the blade approached the region over the wing, the inflow was made to decrease sinusoidally to 80% of the constant inflow velocity. The inflow was made to be symmetric about the center point above the wing. The following blade element algorithm was developed for determining the inflow as the blade passed through the fountain:

The distance from the wing center to the edge of the fountain was defined as:

$$\text{CHALF} = \frac{\text{RK1}}{2} \cdot \text{wing chord} + \frac{\text{RK2}}{2} \cdot \text{wing chord}$$

and the width of the half sinusoid in the entry of the fountain was defined as:

$$\text{WHALF} = \text{RK2} \cdot \text{wing chord}$$

Where RK1 and RK2 are two defined constants. For the case of the sharp fountain, RK1 = 0.5 and RK2 = 0.1, and thus CHALF = 0.3·wing chord and WHALF = 0.1·wing chord. For the smooth fountain, RK1 = 0.5 and RK2 = 0.5, and thus CHALF = 0.5·wing chord and WHALF = 0.5·wing chord. For a given blade element at a radial distance r from the hub, the fountain intensity is defined by four azimuthal angles: PSI1, the angle swept out as the blade element rotates from the aircraft axis of symmetry to where the leading edge intersects the edge of the fountain defined by CHALF, PSI2, the angle swept out as the blade element rotates from the aircraft axis of symmetry to where the leading edge intersects the end of the fountain entrance defined by CHALF - WHALF, PSI3, and PSI4 which are the mirror image of PSI2 and PSI1 over the mid-chord of the wing. In summary:

$$\begin{aligned} \text{PSI1} &= \cos^{-1}\left(\frac{\text{CHALF}}{r}\right) \\ \text{PSI2} &= \cos^{-1}\left(\frac{\text{CHALF} - \text{WHALF}}{r}\right) \\ \text{PSI3} &= \cos^{-1}\left(\frac{\text{WHALF} - \text{CHALF}}{r}\right) \end{aligned}$$

$$\text{PSI4} = \cos^{-1}\left(\frac{-\text{CHALF}}{r}\right)$$

The fountain effect was numerically modeled by decreasing the inflow velocity seen by the blade element, V_{inf} , as it passes through the fountain in the following manner ($rpsi$ is the azimuthal position of the blade element and AMP is the maximum fractional decrease of V_{in}):

$$\text{PSI1} \leq rpsi \leq \text{PSI2}; \quad V_{inf} = V_{in} \cdot \left[1 - \text{AMP} \cdot \sin\left(\frac{rpsi - \text{PSI1}}{\text{PSI2} - \text{PSI1}} \frac{\pi}{2}\right)\right]$$

$$\text{PSI2} < rpsi \leq \text{PSI3}; \quad V_{inf} = V_{in} \cdot (1 - \text{AMP})$$

$$\text{PSI3} < rpsi \leq \text{PSI4}; \quad V_{inf} = V_{in} \cdot \left[1 - \text{AMP} \cdot \cos\left(\frac{rpsi - \text{PSI3}}{\text{PSI4} - \text{PSI3}} \frac{\pi}{2}\right)\right]$$

In the model used for the current calculations, $\text{AMP} = .2$, reflecting the 20% decrease in inflow at the mid-chord of the wing. At all other azimuthal positions, no change was made in the inflow velocity, thus the total inflow is not fully consistent with that required by momentum analysis.

Appendix E

Rotor and Blade Properties

Station Number	Radial Station r/R	ft	Chord (ft)	Thickness Ratio t/c	Twist degrees	Air Foil Section
1	0.00	0.00	1.5167	0.35	0.00	NACA 64-935
2	0.17	2.15	1.2771	0.28	-10.392	NACA 64-528
3	0.19	2.33	1.2567	0.27	-11.278	*
4	0.25	3.13	1.1667	0.26	-15.104	*
5	0.40	5.00	1.1667	0.21	-24.167	*
6	0.45	5.63	1.1667	0.20	-26.337	*
7	0.50	6.25	1.1667	0.19	-29.130	*
8	0.53	6.63	1.1667	0.18	-29.922	NACA 64-118
9	0.60	7.50	1.1667	0.17	-31.771	*
10	0.70	8.75	1.1667	0.14	-34.413	*
11	0.81	10.13	1.1667	0.12	-37.318	NACA 64-(1.5)12
12	0.91	11.31	1.1667	0.10	-39.827	*
13	0.95	11.88	1.1667	0.09	-41.016	*
14	1.00	12.50	1.1667	0.08	-42.337	NACA 64-208

* Properties vary uniformly between stated values

Rotor

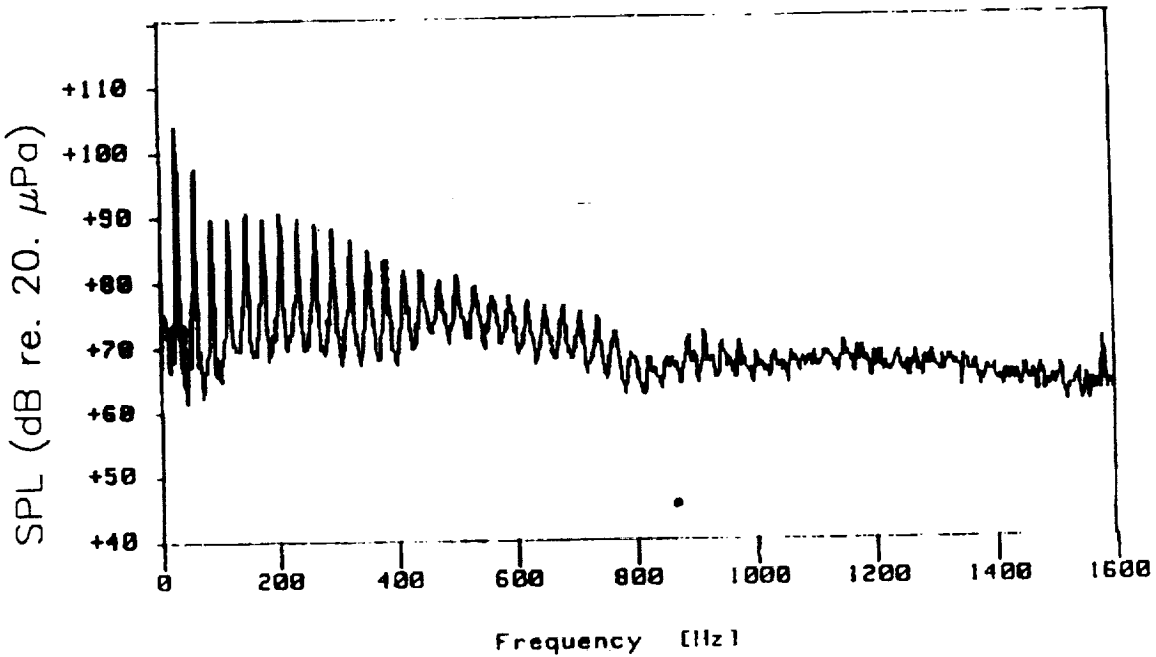
Number of blades per rotor	3
Diameter	25.0 ft
Disc area per rotor	491 sq. ft
Solidity	0.089
Hub precone angle	2.5 degrees
Blade Lock number	3.83
Blade cut out radius	1.06 ft

Operating Conditions

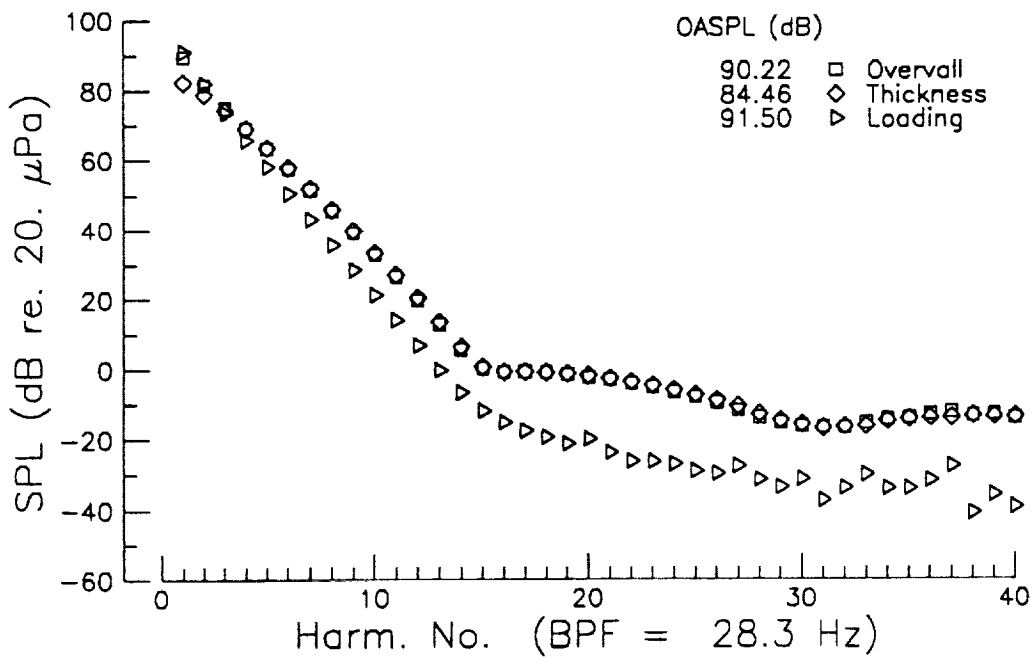
	<u>Hover</u>	<u>Forward Flight</u>
Speed of sound	343.0 m/s	343.0 m/s
Ambient density of air	1.21 kg/m ³	1.21 kg/m ³
Angle of descent	0 degrees	0 & 6 degrees
Observer distance to rotor	60.8 m	152.4 m
Elevation angle	10.81 degrees	90 degrees
Coefficient of thrust	0.0091	0.0072
Rotor RPM	565	565
Nacelle angle	90 degrees	90 degrees
Aircraft gross weight	13000 lb	13000 lb

References

1. Bretner, Kenneth S. (1986). *Prediction of Helicopter Rotor Discrete Frequency Noise : A Computer Program Incorporating Realistic Blade Motions and Advanced Acoustic Formulation*, NASA Technical Memorandum 87721, October 1986.
2. Maisel, M. (1975). *Tilt Rotor Research Aircraft Familiarization Document*, NASA Technical Memorandum X-62, 407, January 1975.
3. Abbott, I. H., and Von Doenhoff, A. E. (1959). **Theory of Wing Sections**. Dover Publications, Inc., New York.
4. George, Albert R., Smith, Charles A., Maisel, Martin D., and Brieger, John T. (1989). *Tilt Rotor Aircraft Aeroacoustics*, Proceedings of the 45th Annual Forum & Technology Display of the American Helicopter Society, Boston, Massachusetts, May 22-24, 1989.
5. Prouty, R. W., (1986). **Helicopter Performance, Stability, And Control**. PWS Publishers, Boston. Chapters 1 & 3.
6. Richards, E. J., Mead, D. J., (1968). *Noise and Acoustic Fatigue in Aeronautics*. John Wiley & Sons, Inc. New York
7. Kuethe, A. M. and Chow, C. Y. (1986). **Foundations of Aerodynamics**. John Wiley & Sons, Inc. New York. pp. 134-136.
8. Stivers, L. S. (1954). *Effects of Subsonic Mach Number on the Forces and Pressure Distributions on Four NACA 64A-Series Airfoil Sections at Angle of Attack as High as 28°*, NACA Technical Note 3162, March 1954.
9. Rutherford, J. W., and Morse, H. A. (1985). *The Tilt Rotor Download Investigation*, Videotape, U. S. Army Aeroflightdynamics Laboratory, 7 x 10 Wind Tunnel, Ames Research Center, July 1985.

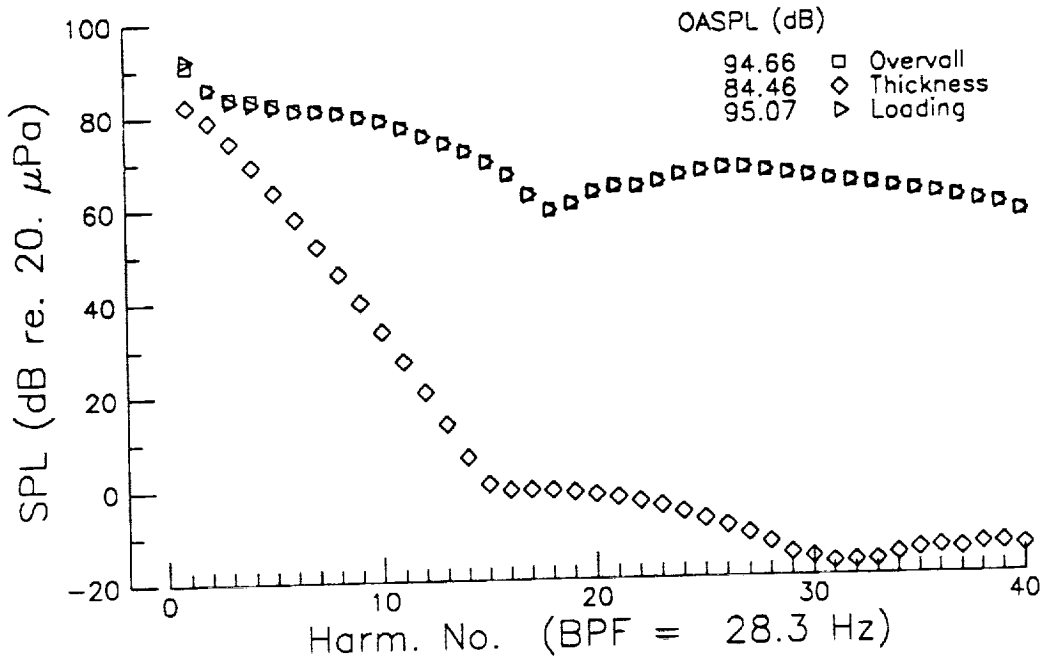


a. Experimental Spectrum. 2 Hz bandwidth.

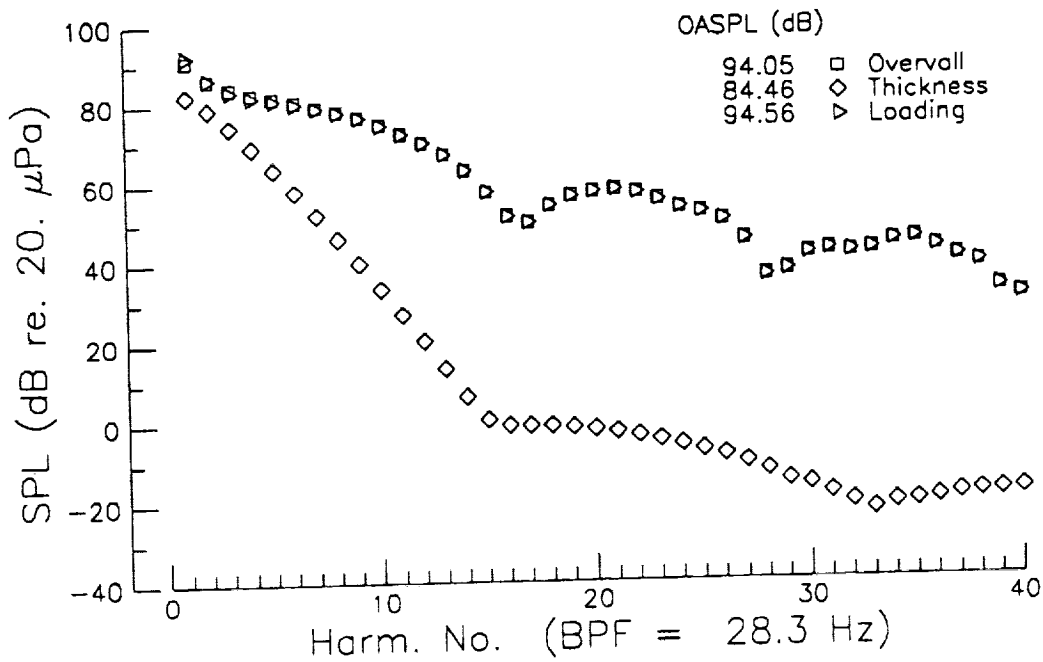


b. WOPWOP calculation, quasi steady model without fountain model.

Figure 1 a-b. Spectra of sound, 0-1600 Hz, for XV-15 hover, 90° nacelle, 98% rpm, 180° azimuth, 25' wheel height altitude, ground plane microphone at 196'.

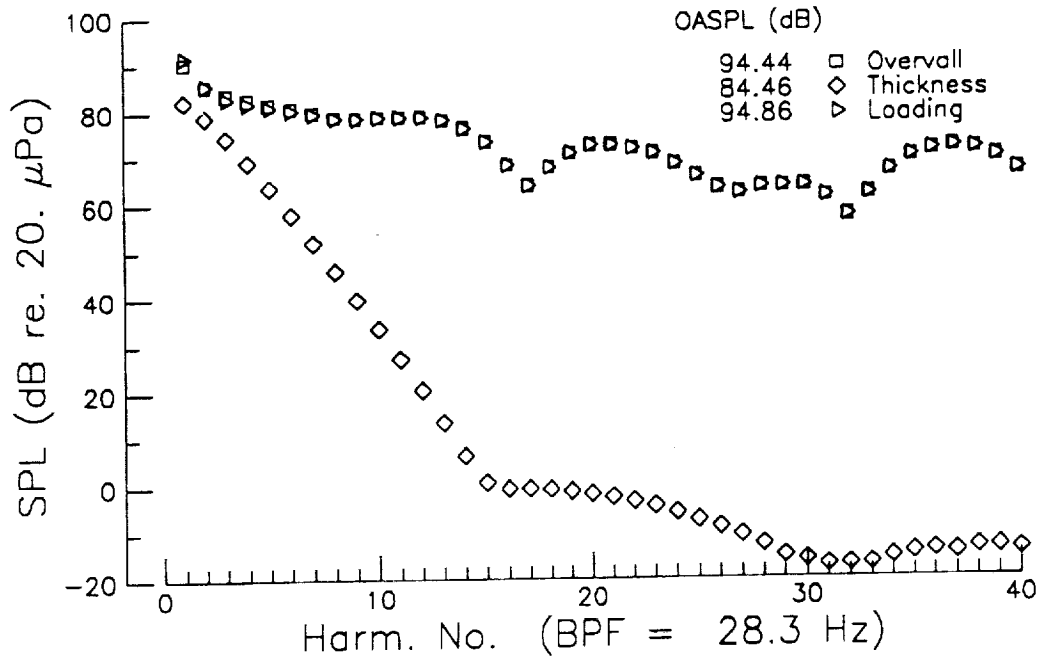


c. WOPWOP calculation, quasi steady model, sharp fountain model.

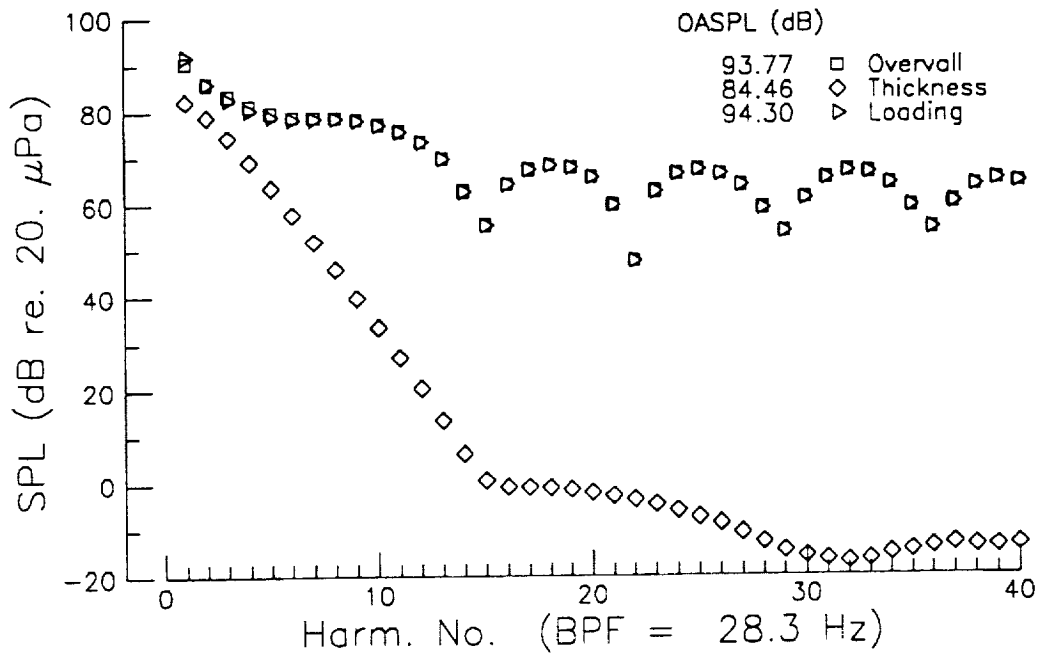


d. WOPWOP calculation, quasi steady model, smooth fountain model.

Figure 1 c-d. Spectra of sound, 0-1600 Hz, for XV-15 hover, 90° nacelle, 98% rpm, 180° azimuth, 25' wheel height altitude, ground plane microphone at 196'.



e. WOPWOP calculation, quasi steady stall model, sharp fountain model.



f. WOPWOP calculation, quasi steady stall model, smooth fountain model.

Figure 1 e-f. Spectra of sound, 0-1600 Hz, for XV-15 hover, 90° nacelle, 98% rpm, 180° azimuth, 25' wheel height altitude, ground plane microphone at 196'.

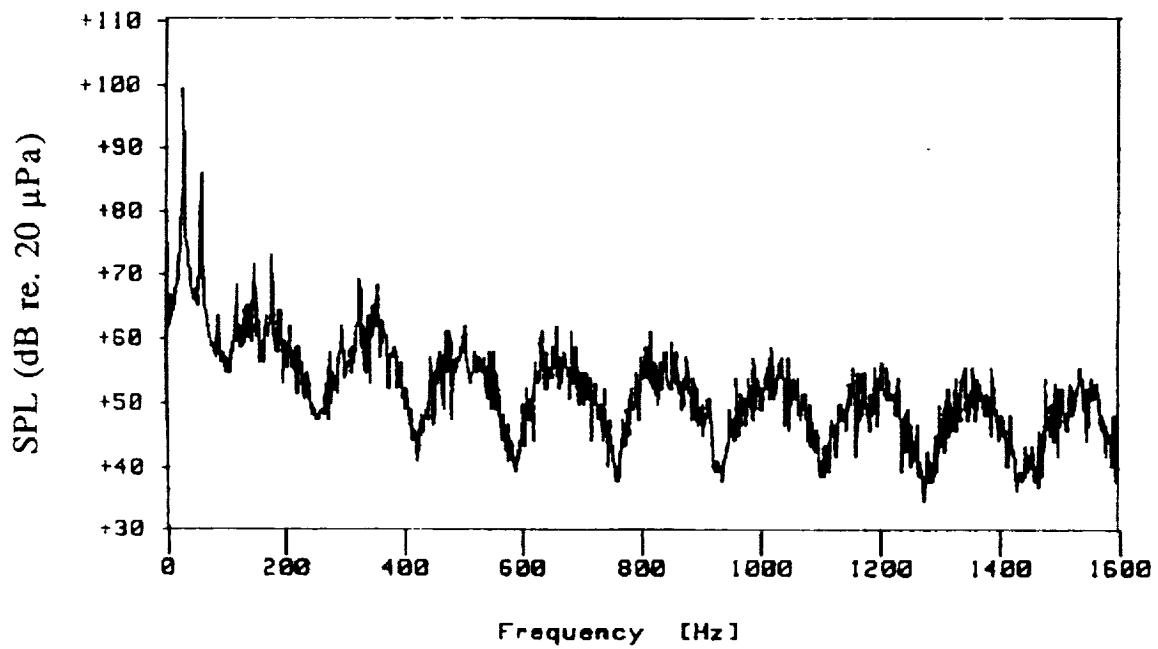
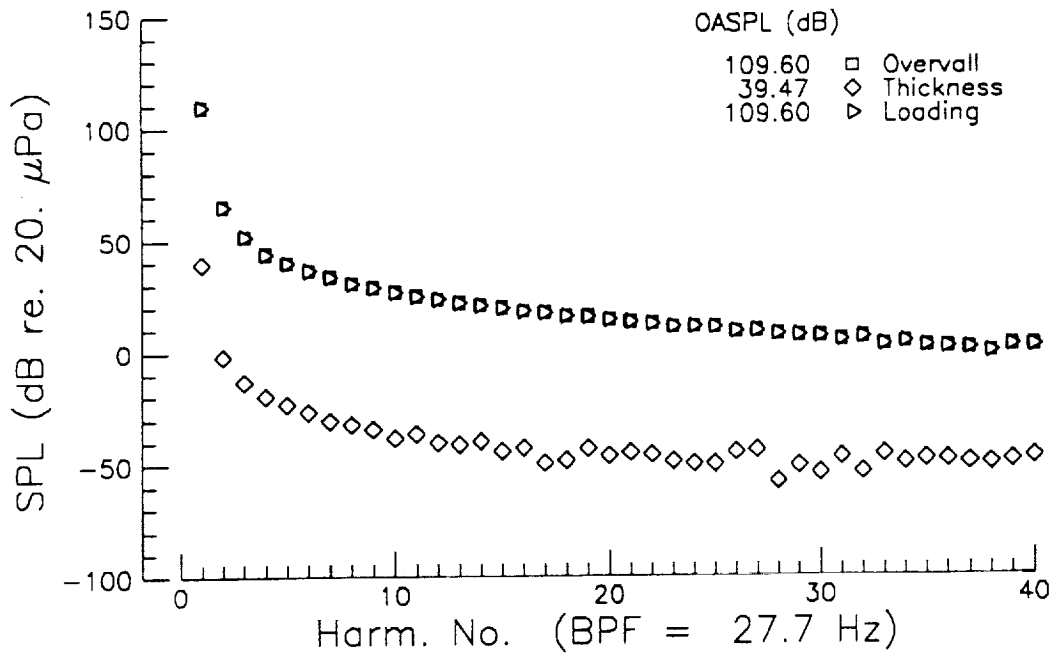
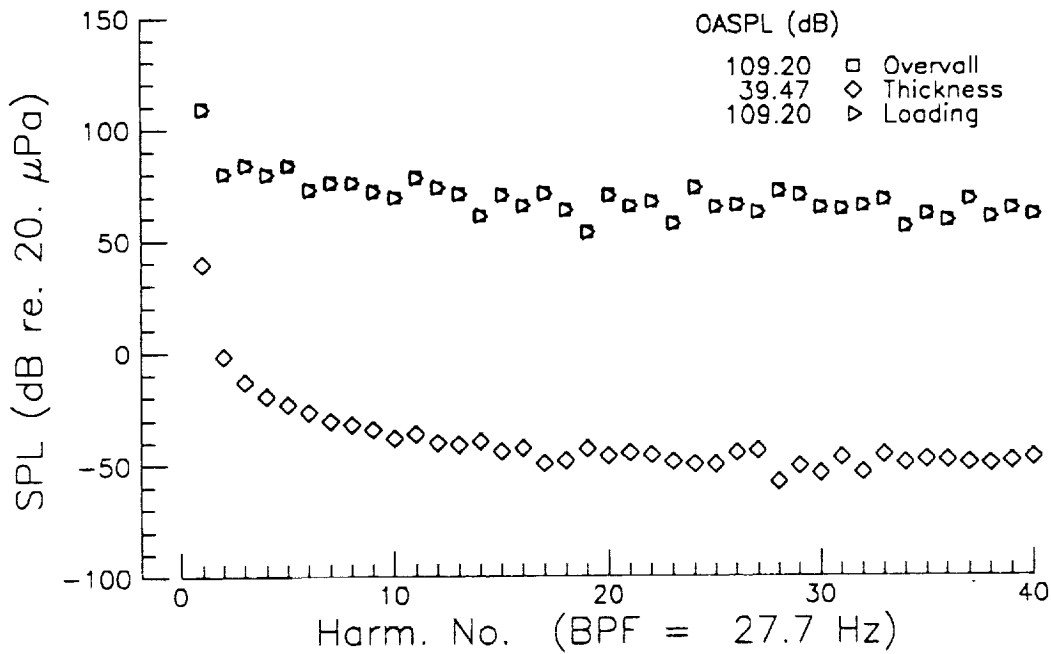


Figure 2 a. Experimental spectrum of sound for XV-15 level flyover, 85° nacelle, 60 knots IAS, $x = 0'$ overhead, $y = 0'$ centerline, $z = 500'$ altitude, 98% rpm, 2 Hz bandwidth.



b. WOPWOP calculation, forward flight model, quasi steady model.



c. WOPWOP calculation, forward flight model, quasi steady stall model.

Figure 2 b-c. Predicted spectra of sound for XV-15 level flyover, 85° nacelle, 60 knots IAS, x = 0' overhead, y = 0' centerline, z = 500' altitude, 98% rpm.

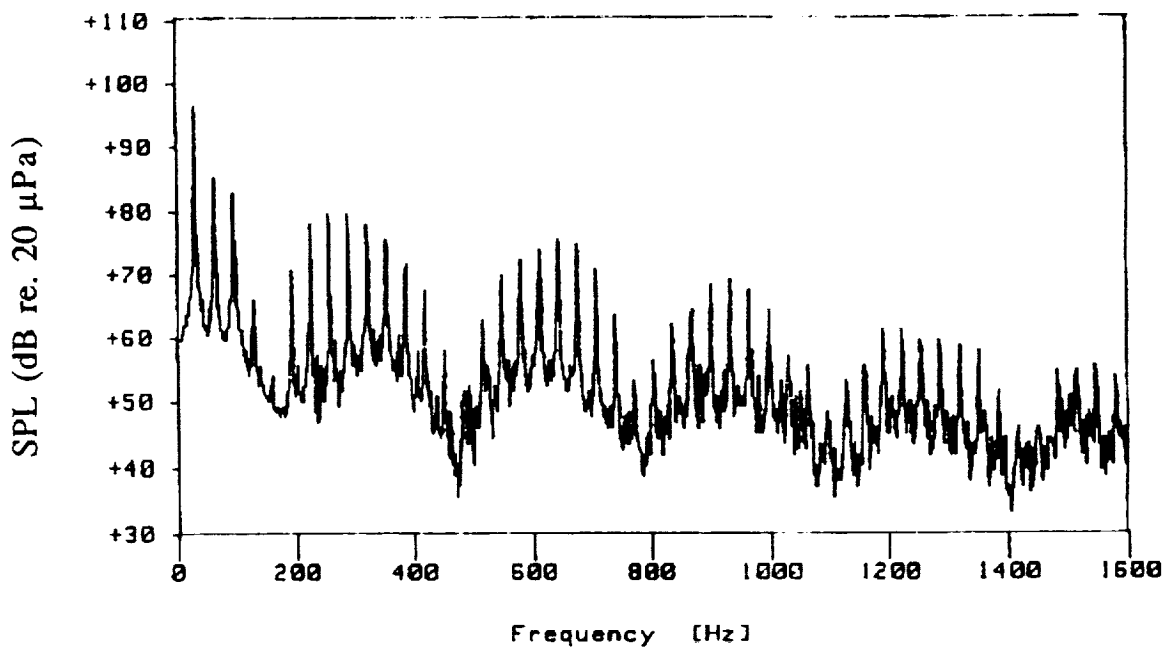
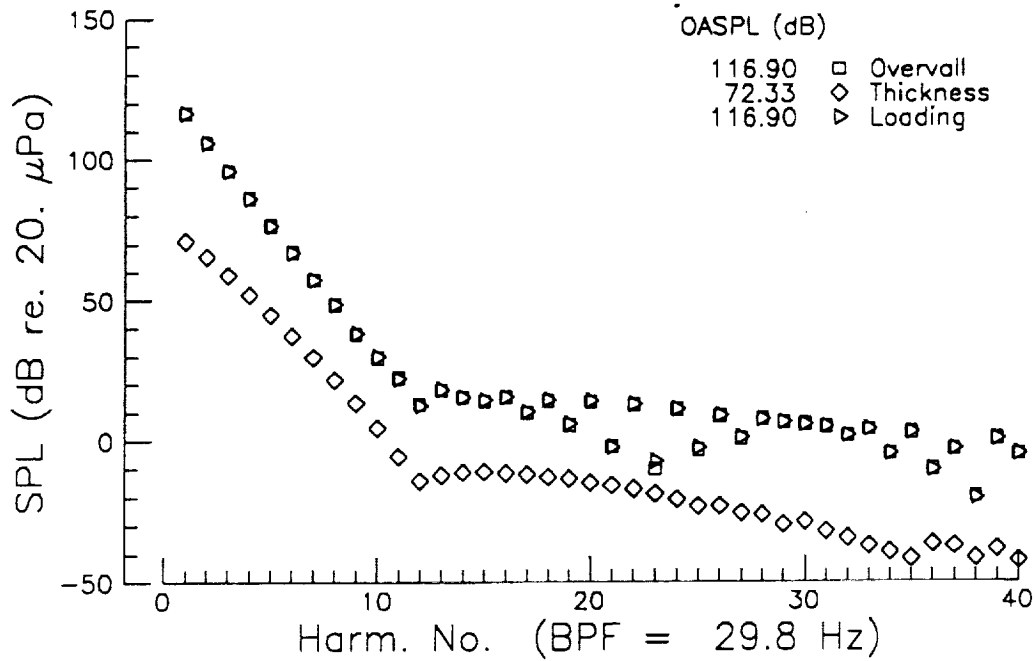
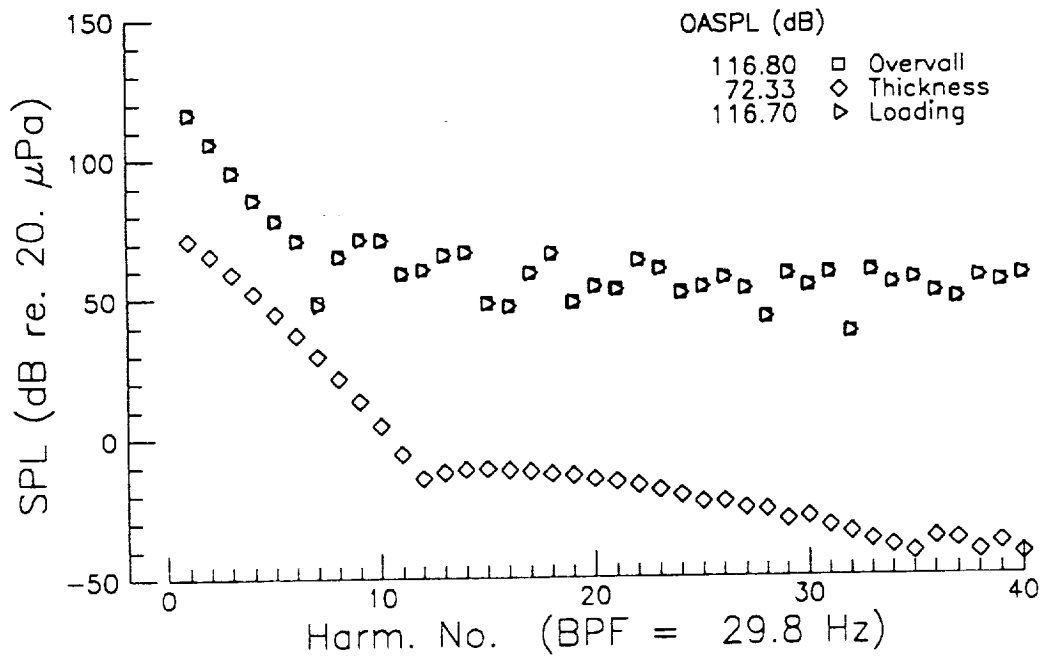


Figure 3 a. Experimental spectrum of sound for XV-15 level flyover, 85° nacelle, 60 knots IAS, $x = -605'$, $y = 0'$ centerline, $z = 500'$ altitude, 98% rpm, 2 Hz bandwidth.



b. WOPWOP calculation, forward flight model, quasi steady model.



c. WOPWOP calculation, forward flight model, quasi steady stall model.

Figure 3 b-c. Predicted spectra of sound for XV-15 level flyover, 85° nacelle, 60 knots IAS, x = -605', y = 0' centerline, z = 500' altitude, 98% rpm.

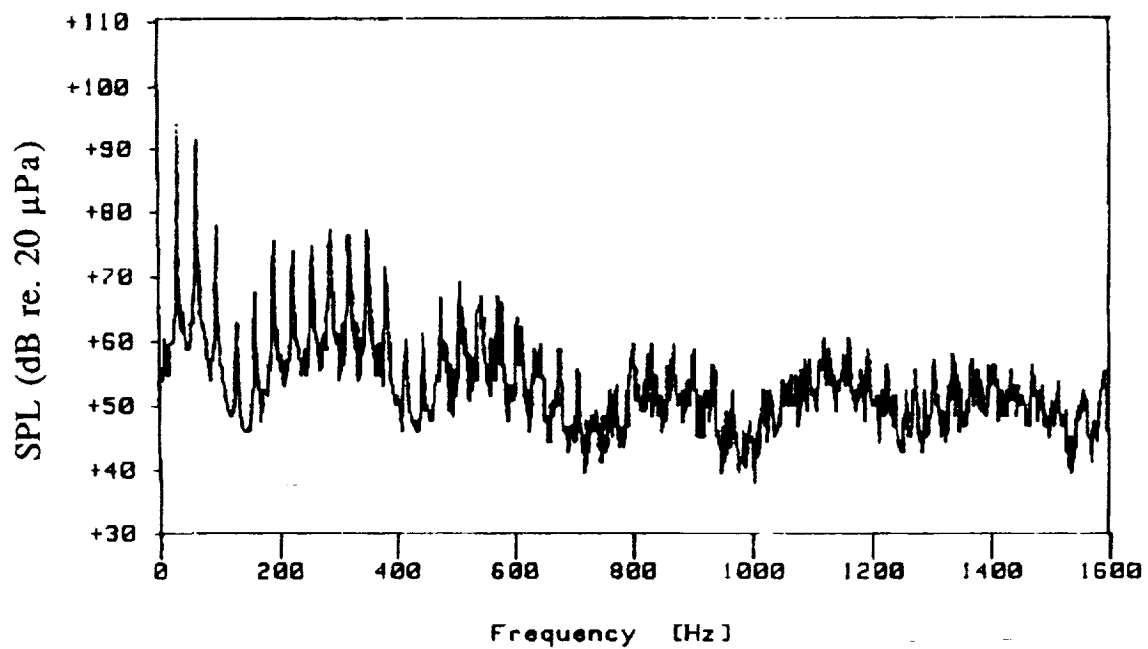
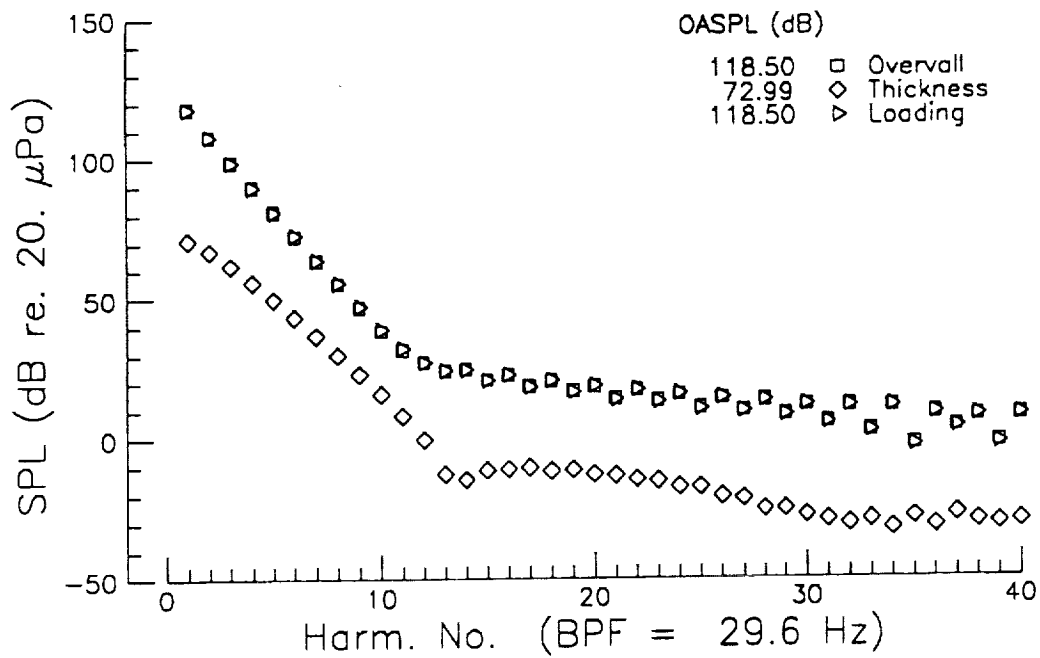
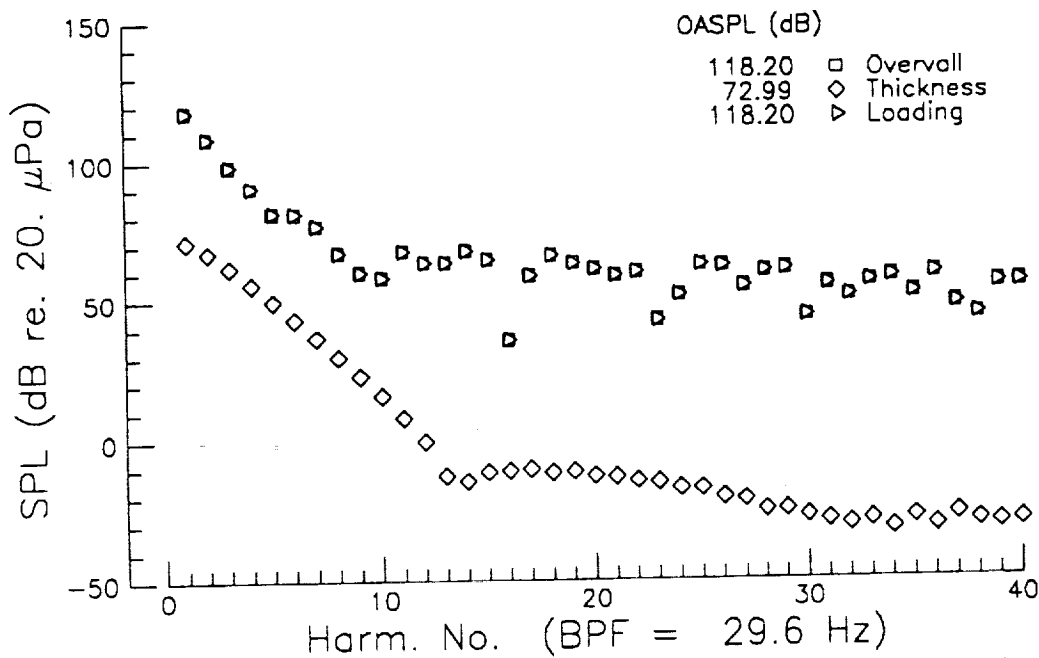


Figure 4 a. Experimental spectrum of sound for XV-15 6° approach, 85° nacelle, 70 knots IAS, x = -435' uprange, y = 500' sideline, z = 400' altitude, 98% rpm, 2 Hz bandwidth.

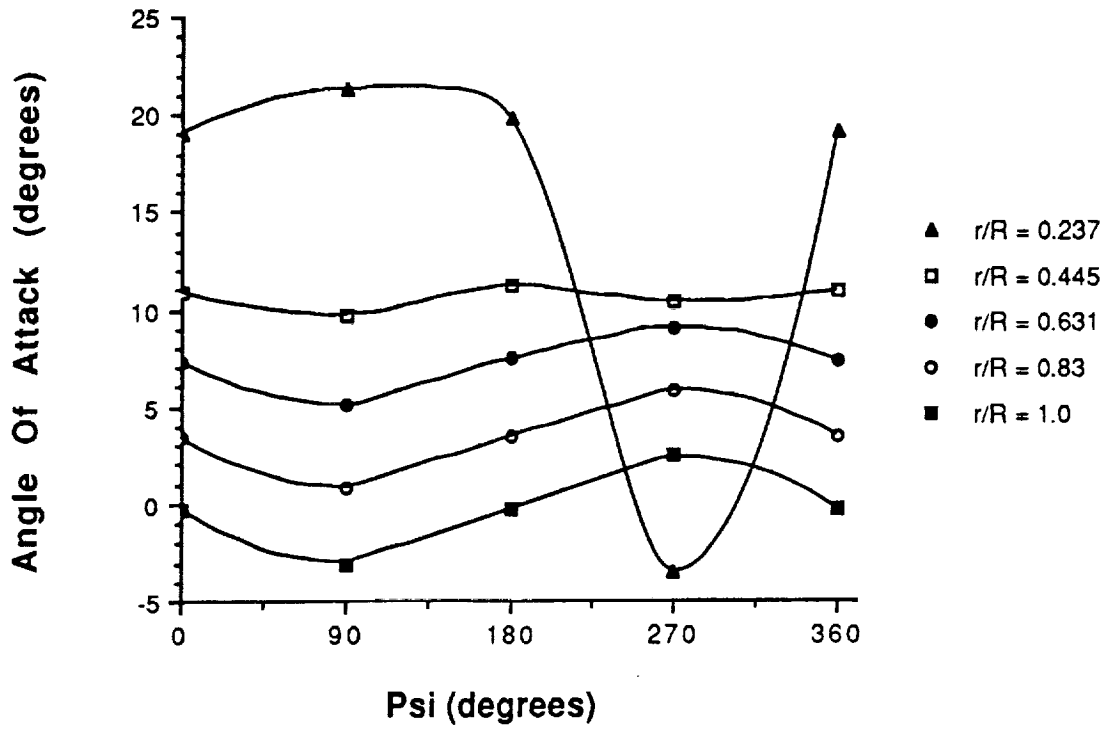


b. WOPWOP calculation, forward flight model, quasi steady model.

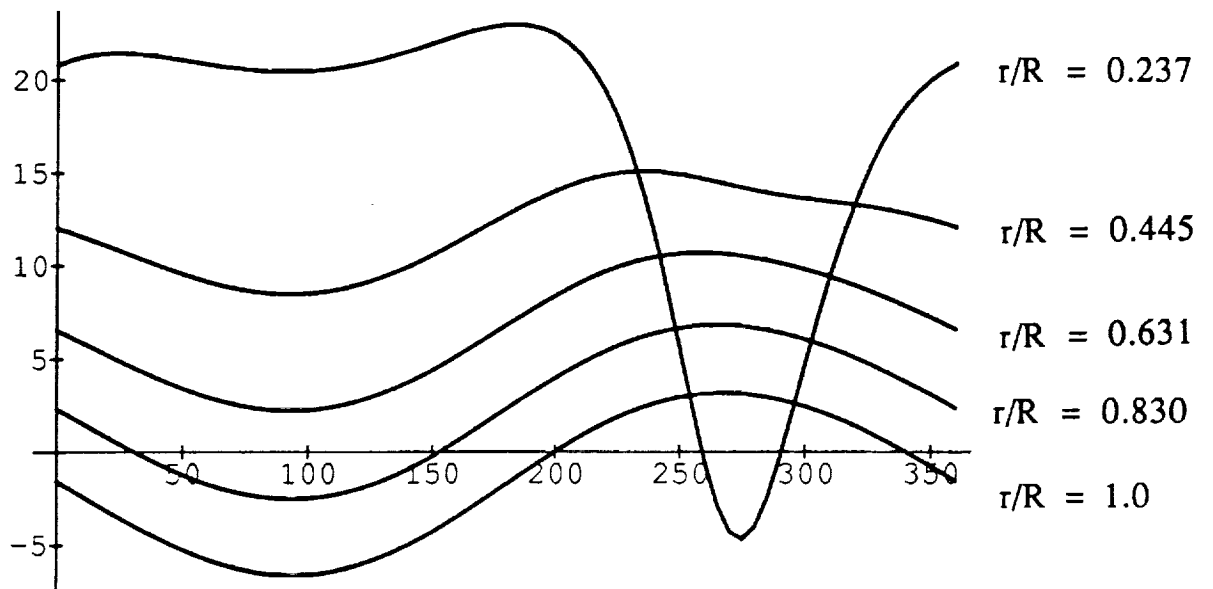


c. WOPWOP calculation, forward flight model, quasi steady stall model.

Figure 4 b-c. Predicted spectra of sound for XV-15 6° approach, 85° nacelle, 70 knots IAS, x = -435' uprange, y = 500' sideline, z = 400' altitude, 98% rpm.



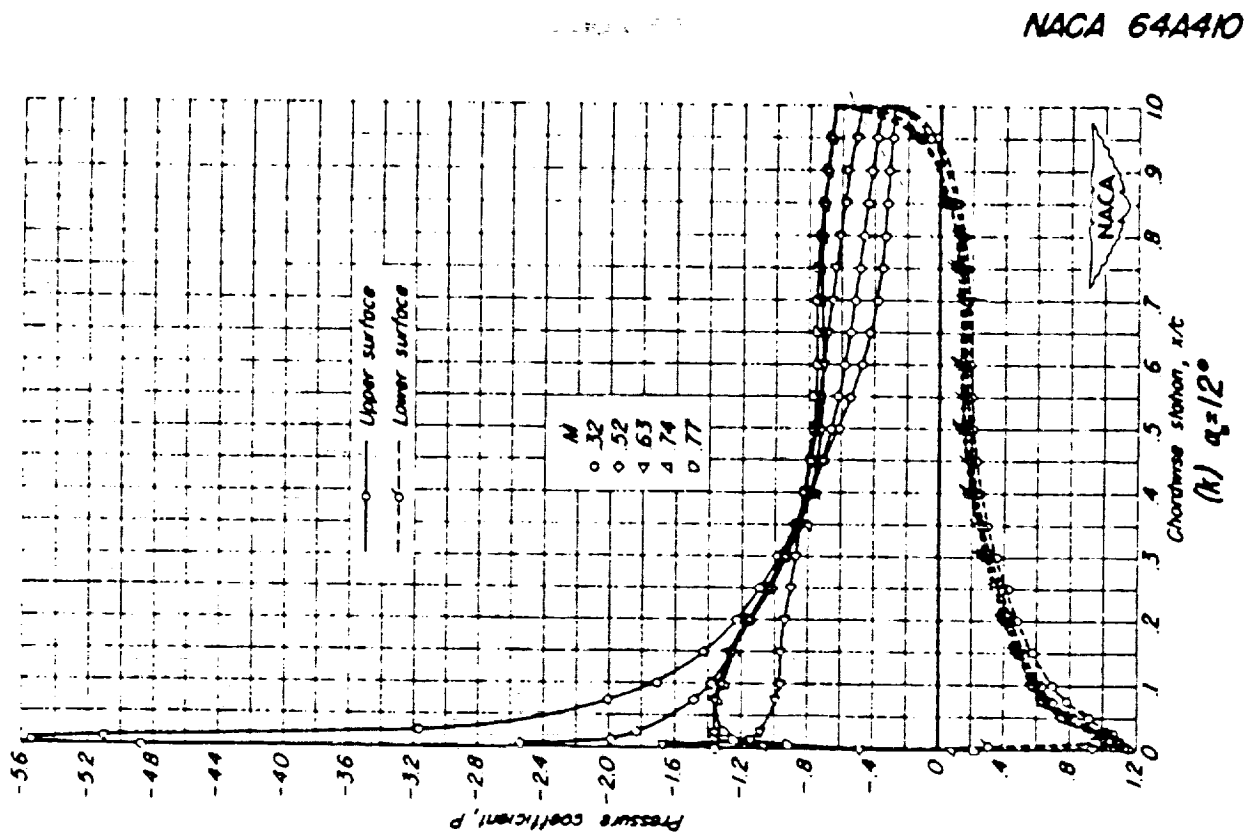
a. Data points provided by Bell.



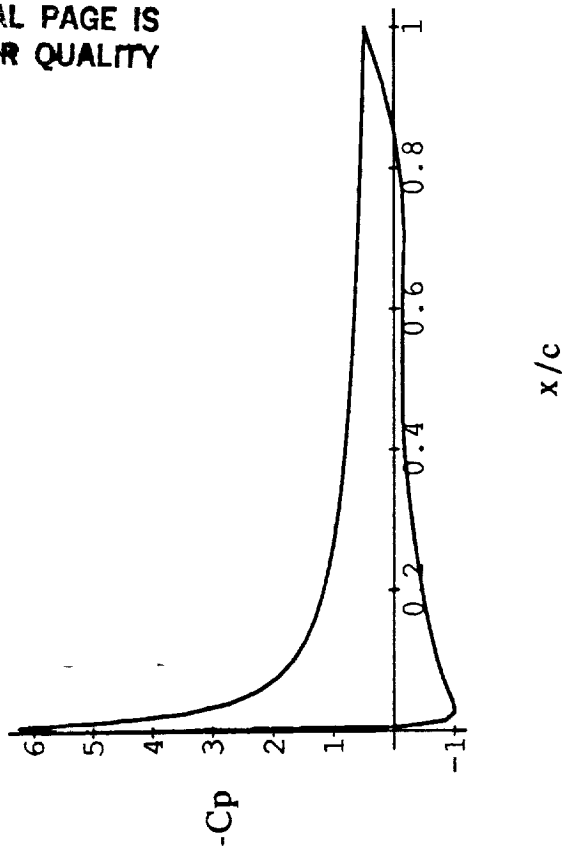
b. Forward flight model used in WOPWOP calculations.

Figure 5 a-b. Angle of attack vs. azimuthal position for 5 radial locations on the rotor blade. 85° degree nacelle, 80 knots IAS, flaps 20°.

Figure 6 a-b. Chordwise pressure distribution for 64A410 airfoils at 12° angle of attack (static).



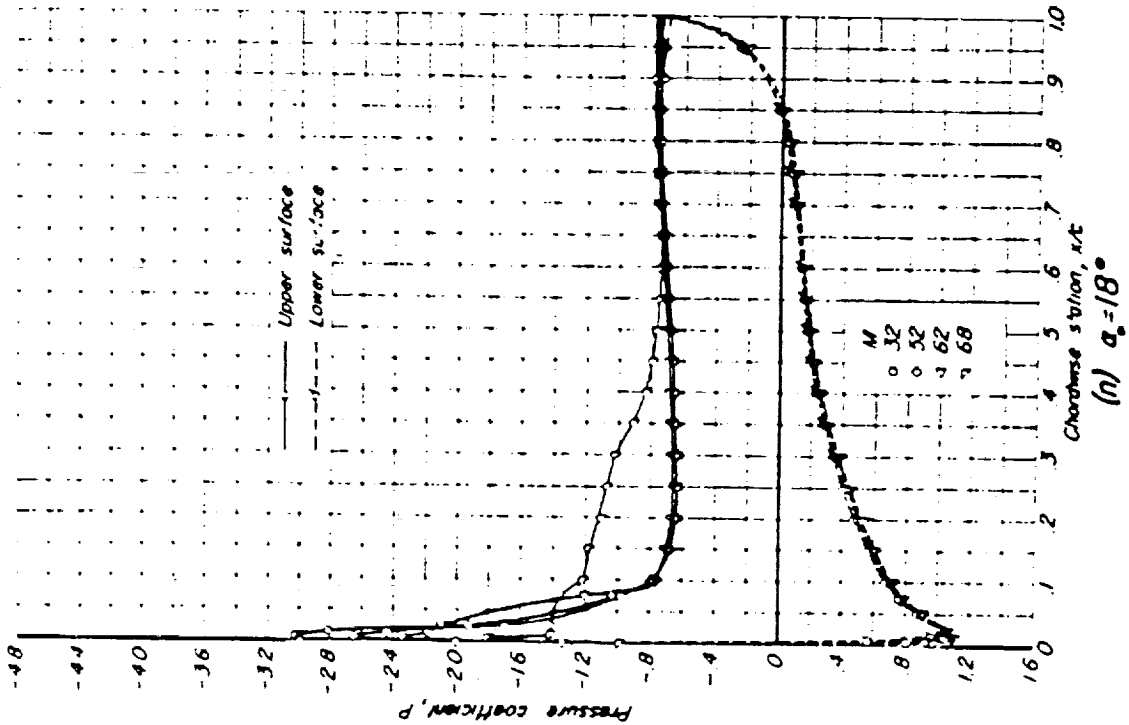
ORIGINAL PAGE IS
OF POOR QUALITY



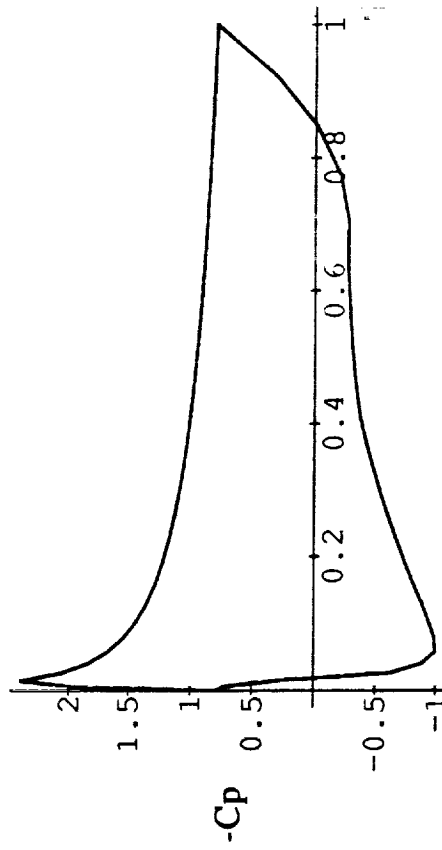
a. Experimental data of reference 8.

b. Mathematical model used in WOPWOP calculations

Figure 6 c-d. Chordwise pressure distribution for 64A410 airfoils at 18° angle of attack (static).



ORIGINAL PAGE IS
OF POOR QUALITY



c. Experimental data of reference 8.

d. Mathematical model used in WOPWOP calculations

ORIGINAL PAGE IS
OF POOR QUALITY

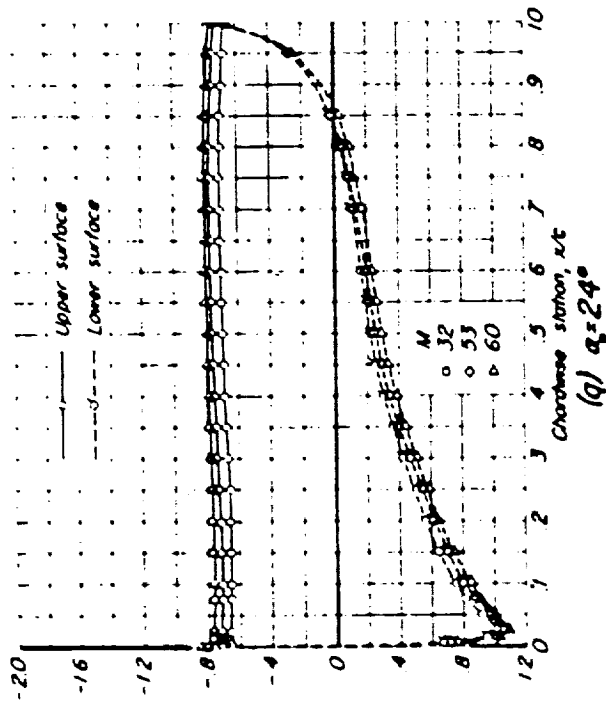


Figure 6 e-f. Chordwise pressure distribution for 64A410 airfoils at 24° angle of attack (static).

e. Experimental data of reference 8.

f. Mathematical model used in WOPWOP calculations

